Retarding Potential Analyser Development for Low Density FEEP Thruster Beam Diagnostics

IEPC-2019-445

Presented at the 36th International Electric Propulsion Conference
University of Vienna, Austria
September 15-20, 2019

Nina S. Mühlich*, Sebastian Keerl†, Werner Engel‡, Emre Ceribas§ and Robert-Jan Koopmans¶
FOTEC Forschungs- und Technologietransfer GmbH, Wr. Neustadt, 2700, Austria

The FEEP-technology has been developed at FOTEC under ESA research contracts as an efficient propulsion technology for future science missions. For further investigation of this technology a plume diagnostics system consisting of several different probes was built including a Retarding Potential Analyser (RPA) for analysing the ion energy distribution. The existing RPA design requirements are derived for higher density thruster plumes. A FEEP thruster beam has a plasma density several orders of magnitude lower compared to other electric propulsion thrusters such as HETs and GITs. RPAs designed for these thrusters are not necessarily suitable for low-density FEEP thruster plumes. For this reason, several different design configurations were tested to find the most suitable design for the FEEP thruster plume. The RPA development process and first measurement results will be presented.

Nomenclature

FEEP	= Field Emission Electric Propulsion	d	= grid aperture distance
GIT	= Gridded Ion Thruster	I_c	= total collector ion current
HET	= Hall Effect Thruster	k_B	= boltzmann constant
IFM	= Indium FEEP Multiemitter	o	= orifice diameter
LIFET	= Large Indium FEEP Test	s	= grid aperture diameter
LMIS	= Liquid Metal Ion Source	T_e	= electron temperature
mN-FEEP	= FEEP with around 1 mN of thrust	V_d	= voltage between two grids
PCB	= Printed Circuit Board	x	= distance between RPA grids
RPA	= Retarding Potential Analyser	λ_d	= Debye length

*Researcher, Aerospace Engineering, Muehlich@fotec.at
†Researcher, Aerospace Engineering, Keerl@fotec.at
‡Researcher, Aerospace Engineering, Engel@fotec.at
§Researcher, Aerospace Engineering, Ceribas@fotec.at
¶Team leader Chemical Propulsion, Aerospace Engineering, Koopmans@fotec.at

I. Introduction

Over the past decade, FOTEC has developed the FEEP-technology operating in the μN thrust range, which makes these thrusters ideal for precision control of a spacecraft. The thruster is based on the liquid metal ion source (LMIS) concept, where liquid metal is used as propellant. The emitter consists of a porous tungsten crown, wetted with liquid indium. A high voltage is applied between emitter and an accelerator electrode, which leads to a strong electric field. Ions are extracted from the needle cone tips and are accelerated in the direction of the extractor electrode and thereby generating thrust. An example is the IFM Nano thruster developed at FOTEC and sold commercially by ENPULSION, which is a thruster module specifically designed for CubeSats. It is important to analyse the properties of a thruster beam, such as the energy distribution of the thruster beam ions. This gives information about the state of charge of the ions or how the energy distribution changes for different thruster beam currents or different positions of the thrust axis. For the development of the Retarding Potential Analyser (RPA) certain design requirements had to be revisited that are only valid for high-density plasmas, whereas the plasma plume of a FEEP thruster has a low-density compared to other electric propulsion thrusters[1]. Therefore, several RPA design configurations were tested. First the distance of the grids was determined and subsequently the influence of the aperture diameter was investigated. Another part of the design development was the determination of suitable potential levels of the retarding and suppressor electrodes.

II. Retarding Potential Analyser Design

A. Design description

RPAs can be categorised as gridded, spherical and single orifice[2]. The current RPA design is based on a gridded design, because it is generally used for relatively low-density plasmas and provides the highest energy resolution. It consists of four grids and a collector, as is shown in Figure 1. The first grid is grounded and prevents the plasma to be affected before reaching the RPA. The second grid is called repeller, because it repels electrons with its negative potential from outside, but allows ions to pass through. The main electrode of the RPA is the retarding electrode. There a positive voltage V_d is swept from 0 V to a higher level than the applied thruster emitter potential to discriminate between ions of different energies. Only ions with an energy higher than eV_d can pass through the retarding electrode and reach the collector. The suppressor is a second negative electrode to prevent secondary electrons, which are generated by ion bombardment, from reaching the collector. This electrode provides a higher resolution of the detected ion current. The last part of the RPA stack is the ion collector, which measures current as a function of the retarding electrode potential. A printed circuit board (PCB) is used to electrically connect the electrical components (grids and collector) and to mechanically fasten them to it. Indium-FEEP thrusters require a very careful diagnostics facility

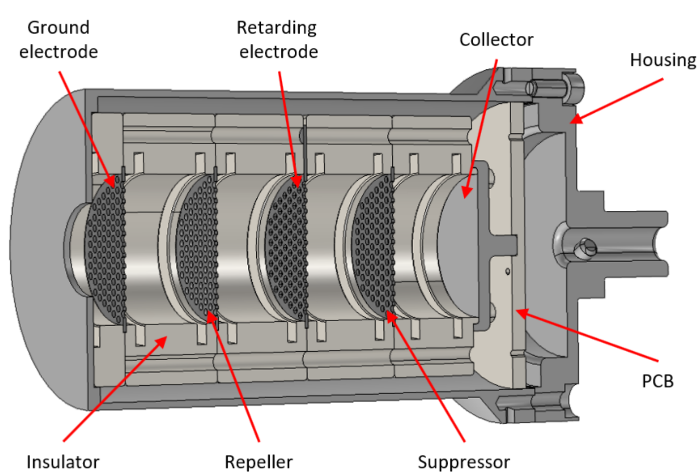

Figure 1. Cut-through of the RPA with indication of its components.

design because nearly all surfaces are covered with indium after having been exposed for some time to the plume[3]. Therefore, the PEEK insulators contain small recesses in which indium can settle and accumulate. The grids were manufactured by laser cutting and are made from stainless steel. An optimum resolution is achieved when the ion trajectories are affected as little as possible. For this reason, the grid apertures are aligned. To ensure their position, all grids have a small extension that fits in a recess in the PEEK insulator. To maximise the transparency, the grid apertures are hexagonally arranged. Spring contact pins provide the electrical contact with the grid electrodes.

B. Design requirements

For the RPA design, certain requirements have to be considered. The energy resolution of the RPA is on the one hand affected by the geometry of the grids and on the other hand by the distance between the grids. Böhm states, that the larger the grid spacing x, the better the ion energy resolution[4]. This is expressed as

$$\frac{\Delta E}{E} \propto \frac{1}{x}. \tag{1}$$

At the same time, however, the larger x the lower the number of ions reaching the collector. In addition, according to Sakai[5], an ion with a certain potential cannot be decelerated by a finite potential difference at an infinitely long distance. Virtual electrodes would be created between the grids by charged particles due to particle collisions. These would cause an axial field and deflect the incident ions, although they have enough energy to pass the retarding electrode. This would cause a shift in energy distribution to lower energies.

Another requirement is that the entrance aperture shall have the smallest diameter in the system[4]. Otherwise, it would lead to ion losses at the RPA insulating walls, because most of the ions enter the RPA at a certain angle with respect to the thrust axis. Additionally, the entrance orifice diameter o should be smaller than the Debye length

$$o < \lambda_d, \tag{2}$$

in order to minimise Debye shielding[6]. Aside from that, the entrance aperture and the grids should be as thin as possible to prevent ion losses to its inner surface and subsequent secondary electron emission[4]. When determining the grid aperture diameter s, it should be considered if the grid aperture diameter would be too high, the potential at the aperture centre would rapidly decay to $\frac{1}{e}$ times that of the grid potential and the particles would pass through a dimple of low potential at the aperture centre. If the grid aperture diameter would be too small, the number of passed particles would be reduced and the signal to-noise-ratio would be too low. So, a trade-off between the two is required. A single orifice-type RPA design would be suitable for high-density plasmas $\left(> 10^{18}\,\mathrm{m}^{-3}\right)$, to avoid space charge limitations between the grids[7]. Sakai[5] proposed a range of grid aperture diameter s and grid aperture distance d for an optimum resolution:

$$0.1 \leq \frac{d}{s} \leq 1. \tag{3}$$

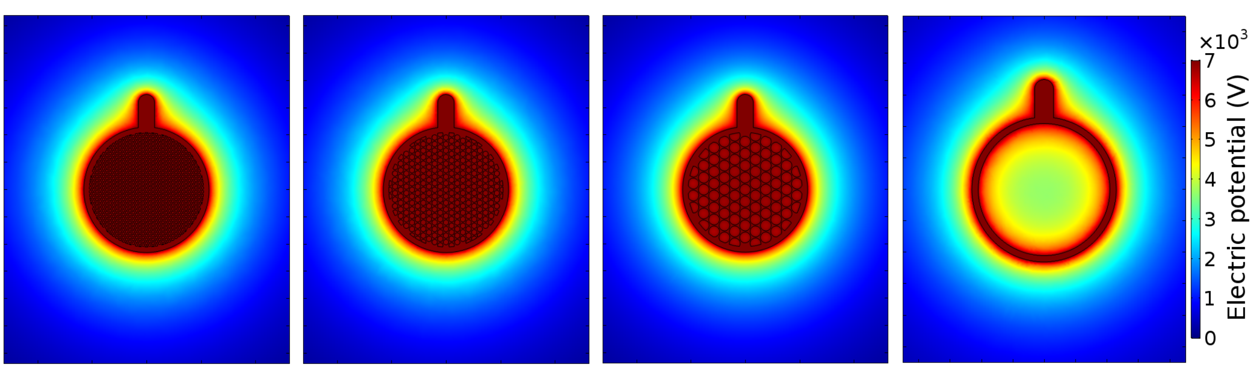

Figure 2. Simulated potential distribution of retarding electrode grids with aperture diameters of (a) 0.5 mm, (b) 1 mm, (c) 2 mm and (d) grid frame, for an applied voltage of 7 kV.

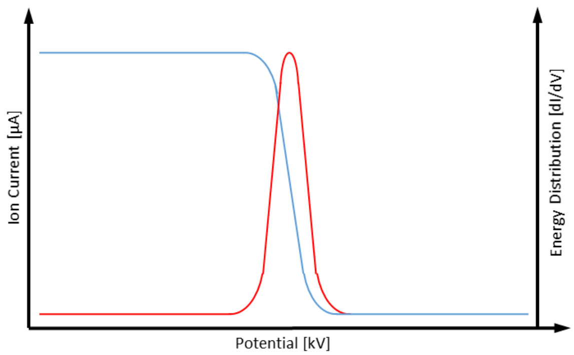

Figure 3. RPA collector signal with ion current (blue) and ion energy distribution (red).

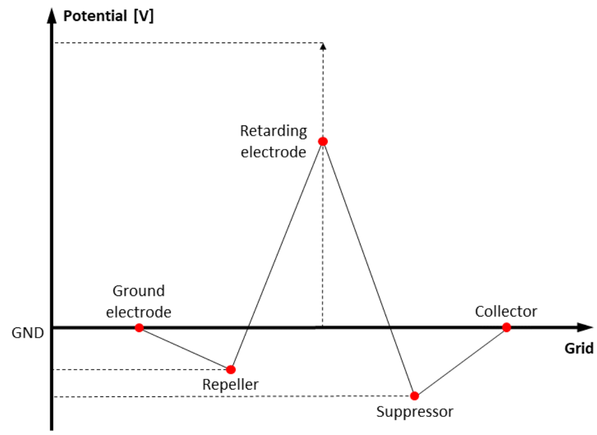

Figure 4. RPA electrode potentials with their position in the RPA electrode stack.

C. Simulation

In section II.B, it is described that ions would pass through a dimple of low potential at the grid aperture centre if the aperture diameter would be too large, which would lead to an inaccuracy of the energy measurement. For analysing this inaccuracy, the potential distribution of the grids was simulated with COMSOL Multiphysics. In Figure 2 the potential distribution of four different retarding electrode grid designs is shown for an applied voltage of 7 kV. It can be seen, that the potential dimple in the centre of an aperture is higher the greater the grid aperture diameter. For example, with a aperture diameter of 1 mm, a potential dimple of around 1 % potential difference occurs. When using a single orifice grid with a diameter of 21 mm, an inaccuracy of around 48 % would occur, which would change the measurement results significantly.

III. Experimental Measurements

A. Setup

The signal from each RPA configuration will be compared to the theoretical signal and its derivative, shown in Figure 3, to find the most suitable design. For the RPA design selection three RPAs were tested simultaneously by measuring the ion beam of the IFM Nano thruster at a distance of 95 cm from the emitted position at an angular separation of 10 ° in horizontal plane in the LIFET4 (Large Indium FEEP Test) facility, as can be seen in Figure 5. In total seven different design configurations were tested, which are listed in Table 1. The configurations differ in their grid spacing and the aperture diameter of the grids. Furthermore, it was necessary to change the thruster parameters and the repeller and suppressor potential.

Table 1. RPA configuration properties and ion thruster settings.

Config.	Grid distance x [mm]	Grid aperture diameter s [mm]	Transparency t [%]	Thruster Parameter	Repeller & Suppressor
c1	5	1	62 %	V_{EM}: 5 kV I_{EM}: 2 mA V_{EX}: 5 kV	R: -15 V S: -20 V
c2	10	1	62 %		
c3	15	1	62 %		
c4	10	0.5	46 %	V_{EM}: 4 kV I_{EM}: 2 mA V_{EX}: 8 kV	R: -30 V S: -35 V
c5	10	2	74 %		
c6	15	0.5	46 %		
c7	15	2	74 %		

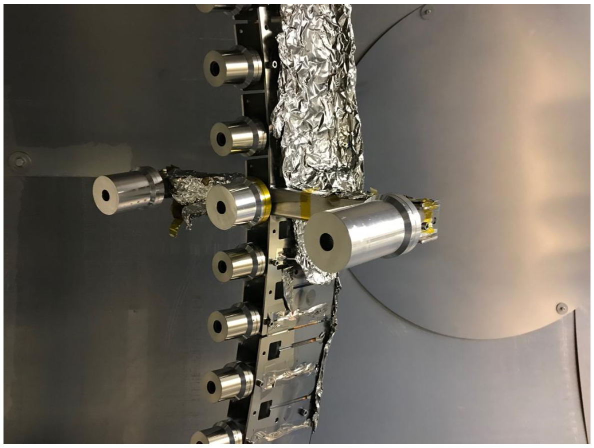

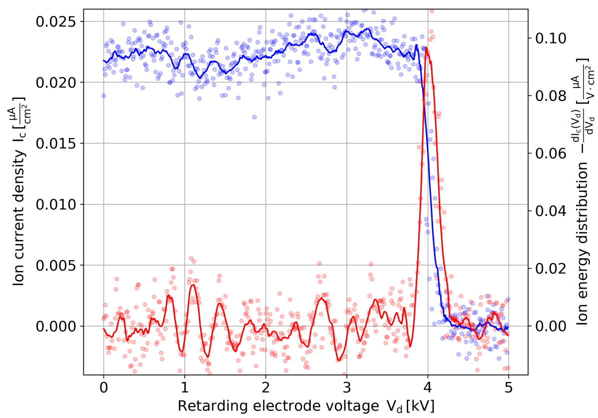

Figure 5. Three RPA configurations mounted horizontally at the centre of the movable diagnostics arm in vacuum facility LIFET4.

Figure 6. Measured ion current density (blue) and its derivative ion energy (red) at 4 kV thruster emitter voltage by using RPA configuration c7.

A qualitative indication of the electrode potential of each grid in the stack is provided in Figure 4. The retarding electrode potential V_d was swept from 0 V to $V_{EM} + 1\,\text{kV}$ with a step size of 10 V. Böhm[4] states that a noticeable deformation of the ion current density measurements would be at sweep rates less than 2 ms. For the measurements a step rate of 100 ms is used. The negative potential grids, i.e. the repeller and the suppressor, are at a constant bias voltage of -30 V and -35 V, respectively. The sweep is conducted at positions of the boom between $-80°$ and $+80\,°$ at increments of $1\,°$. Note that due to the arrangement of the RPAs, one of the RPAs took measurements between -90 ° and +70 °, one between -70 ° and +90 ° and one between -80 ° and +80 °.

B. Measurement results and discussion

In Figure 6 the measurement results of RPA configuration c7 at a thruster emitter voltage V_{EM} of 4 kV is shown. The retarding electrode is used to produce a current-voltage trace (blue line), by sweeping the electrode potential V_d from 0 to 5 kV. The collected current is divided by the collection area to obtain the ion current density and compensated for the different grid transparencies. The total number of ions is collected in the range from 0 to 3.9 kV and sharply decreases until no ions are collected anymore. The red line is the ion current density derivative, plotted as a function of V_d, which shows the ion energy distribution

$$f(eV_d) \propto -\frac{dI_c}{dV_d}, \tag{4}$$

where e is the electronic charge, I_c is the total ion current on the collector and V_d the voltage of the retarding electrode. Here it can be seen, that the energy of the measured ions is around 4 kV, like the applied thruster emitter voltage. As the raw data (indicated by circles) is rather noisy, a Savitzky-Golay filter with a window size of 31 and a polynomial order of 2 is applied to create the line graphs and to be able to compute the derivative of the ion current density. A measured offset for every RPA position is subtracted from the measurements.

Negative potential grids

In the RPA electrode stack two negative electrodes are included. The first negative electrode, the repeller, repels electrons from outside and recaptures secondary electrons which are generated by ion bombardment. The second negative electrode, the suppressor, prevents secondary electrons that are generated by ion bombardment on the grids from reaching the collector. The bias of the suppressor should be more negative than that of the repeller, to accelerate secondary electrons in the direction of the plasma, outside of the probe. In addition, the difference in bias between the suppressor and the repeller prevents secondary electrons to bounce back and forth between the grids, which could lead to ionisation of neutral gas molecules between the grids. As a first analysis it was measured how the measurements would change if no negative electrode would be used.

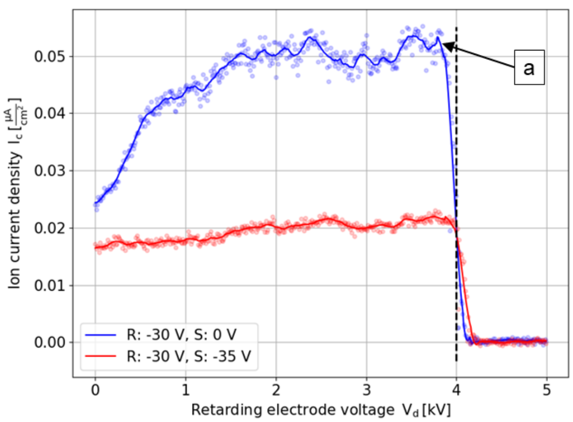

Figure 7. Comparison of measured ion current density for different suppressor potentials.

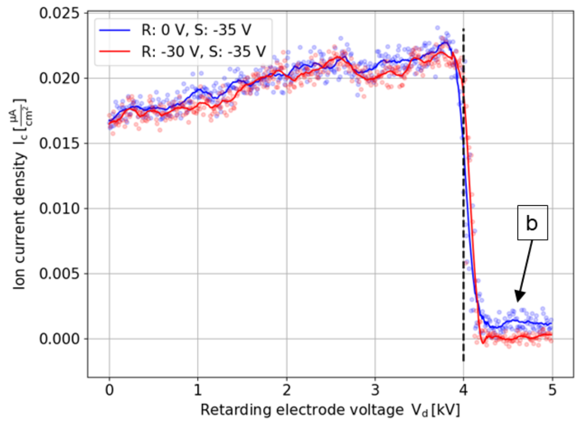

Figure 8. Comparison of measured ion current density for different repeller potentials.

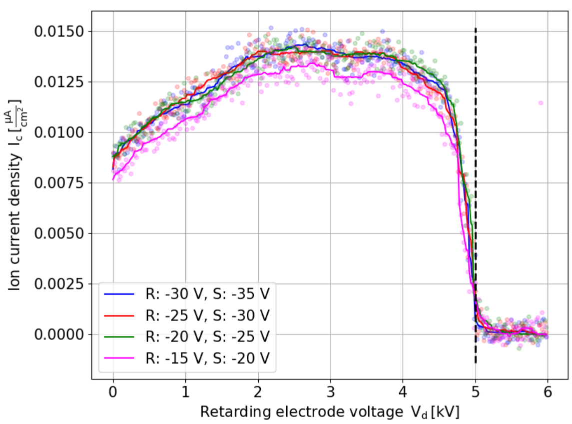

Figure 9. Variation of repeller and suppressor voltages for configuration c3.

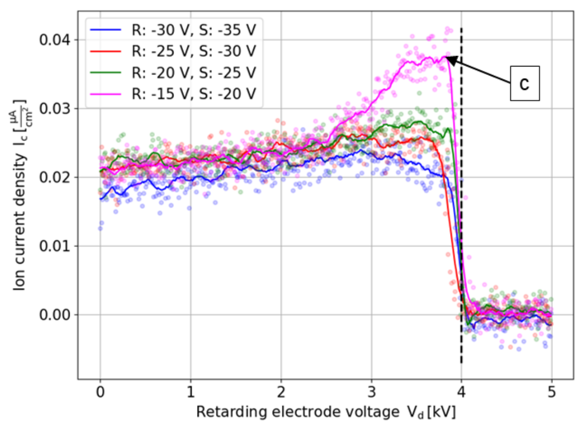

Figure 10. Variation of repeller and suppressor voltages for configuration c7.

The influence of the suppressor is clearly shown in Figure 7. The red line with the suppressor at a negative potential is nearly constant in the area of zero ion energy, so in the range from 0 to 3.9 kV of the retarding electrode. With a suppressor at ground potential an increasing current density is measured (a). At this state, secondary electrons generated by ion bombardment at the collector oscillate along the analyser axis[4]. This effect leads to an increase in the measured current density in region of zero ion energy.
A comparison between the repeller at ground potential and at negative potential can be seen in Figure 8. By applying a higher potential at the retarding electrode than the maximum ion energy, the measured ion current density should be zero. It can be seen that the measured ion current density with a repeller at ground potential never reaches the zero-current level (b). This higher ion current density level is created by electron-neutral collisions[4]. By using a repeller bias of -30,/V this effect is suppressed.
To determine the most suitable biases for the repeller and the suppressor, different voltage settings were tested. Figure 9 shows the results for configuration c3, i.e. a grid distance of 15 mm and a grid aperture diameter of 1 mm. It can be seen that there is no change in the measurement signal by changing the repeller or suppressor voltage. The same measurements were repeated for configuration c7. In this configuration the grid aperture diameter is 2 mm and the grid distance is still 15 mm. Figure 10 shows the results of these measurements. Here the influence of different bias settings of the repeller and suppressor is visible. The more negative the applied repeller and suppressor voltage the more flattened is the signal at the zero ion energy range (c) (Figure 3). For this reason, for the following measurements the repeller and suppressor voltage was set to -30 V and -35 V, respectively. By using different thruster parameter settings, the voltages should be determined again.

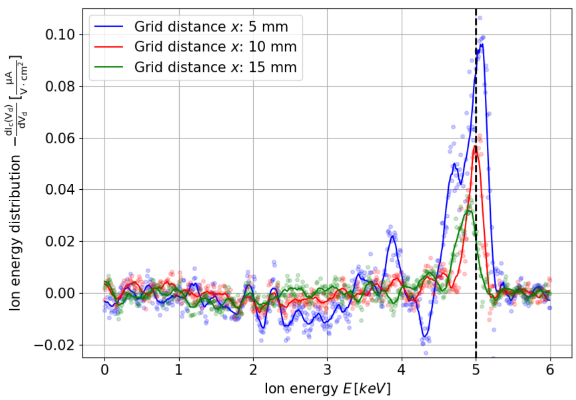

Figure 11. Comparison of ion energy distribution of RPAs with different grid distances and constant grid aperture diameter (s=1 mm).

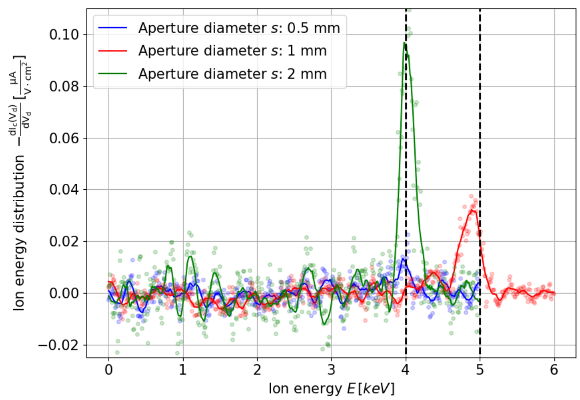

Figure 12. Comparison of ion energy distribution of RPAs with different grid aperture diameters and constant grid distance (x=15 mm).

Grid design

Three different grid distance designs (configuration c1 to c3) were tested with the same grid aperture size of 1 mm at a thruster emitter voltage of 5 kV. The derivative of the current density measurements can be seen in Figure 11. The RPAs with the larger grid distances (configuration c2 and c3) have one maximum in the area of the thruster emitter voltage. The signal of the smallest RPA (configuration c1) has two peaks at different voltages. This is because the grid distance is too small. As described in section II.B the smaller the grid distance, the worse the ion energy resolution $\frac{\Delta E}{E} \propto \frac{1}{x}$ [6]. For configuration c1 (blue line) this is: $\Delta E \propto \frac{5\,\mathrm{kV}}{5\,\mathrm{mm}} = 1\,\frac{\mathrm{kV}}{\mathrm{mm}}$. Due to the fact that the grid aperture diameter is 1 mm, the analyser resolution is $5\,\mathrm{kV} \pm 0.5\,\mathrm{kV}$. Note that the distance between the peaks for this configuration is smaller than the resolution of the RPA. Compare this to the resolution of configuration c3, i.e. for a grid distance of 15 mm. Here the resolution is $5\,\mathrm{kV} \pm 0.17\,\mathrm{kV}$. As described in section II.B, if the grid distance is too large a shift of the ion energy peak to lower energies could be measured. A shift of around 100 V towards lower energies can be seen for configuration c3 (green line) with a grid distance of 15 mm.
With the grid distance selected, the influence of the grid aperture size was investigated. The results are shown in Figure 12. Due to continuous electrical discharges between the grids of configuration c1, the emitter voltage was reduced from 5 kV to 4 kV. In Figure 12 it is shown that the current at the applied thruster emitter voltage is higher for an increasing aperture size. This increase is related to a more precise alignment of the four grids with a higher aperture size, which leads to a better total transparency. Furthermore, it can be seen that the energy shift disappears with a larger aperture size. Therefore, both grid distances, 10 mm and 15 mm can be used with a aperture size of 2 mm. The ion energy angle distribution is presented in Figure 13 for configuration c7. A voltage sweep of the retarding electrode from 0 to 5 kV was carried out at every angle between -70° to +70° in the horizontal plane. It can be clearly seen, that the ion energy is distributed around the applied thruster emitter voltage of 4 kV. Furthermore, the number of detected ions decreases in the direction of the chamber walls.

IV. Conclusion

Seven different RPA configurations based on theoretical design requirements were tested, to find the most suitable design for low-density ion beams of indium FEEP thrusters. The design variation included different grid distances and grid aperture diameters. Furthermore, different operation points of the negative grids repeller and suppressor, were analysed. Based on the results presented above configurations c5 and c7 were identified as the most suitable design configurations. This entails an RPA design where the grid aperture diameter is 2 mm with a grid distance of 10 mm or 15 mm. Depending on the thruster operating point, a compromise can be found between higher energy resolution and the amount of ion current to be measured. If a better energy resolution should be achieved a grid distance of 15 mm is more qualified and for low thruster

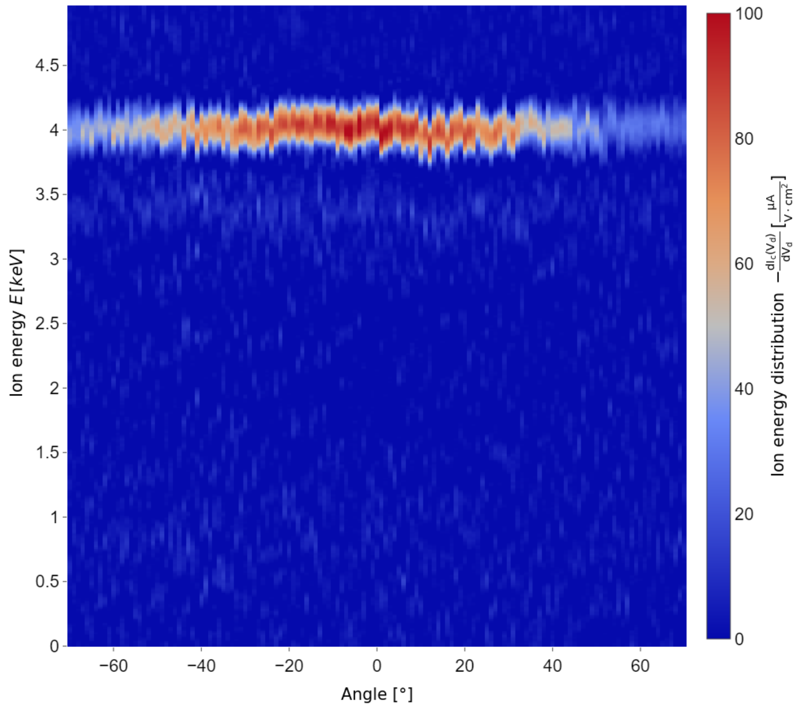

Figure 13. Ion energy angle distribution at thruster emitter voltage of 4 kV measured with configuration c7.

emitter currents a grid distance of 10 mm should be used. In the future, the IFM Nano thruster beam will be analysed more in detail, for example the state of charge of the ions and how the energy distribution changes for different thruster beam currents or for different angles around the thruster.

Acknowledgments

This research has been supported by the "IFM Nano Thruster Module" project, contract number 4000116898/16/NL/EM under the ARTES 5.2 program framework.

References

[1]S. Keerl, D. Jelem, N. S. Mühlich, W. Engel, J. Fries, E. Ceribas, R.-J. Koopmans and B. Seifert, "Two-dimensional plasma plume density characterisation of the IFM Nano Thruster", IEPC-2019-566, 36th IEPC, Austria, 2019.

[2]J. Partridge and N. A. Gatsonis, "Characterization of High-Density Flowing Plasmas Using a Directional Micro-Retarding Potential Analyzer", IEPC-2005-170, 29th IEPC, US, 2005.

[3]M. Tajmar, K. Marhold and S. Kropatschek, "Three-Dimensional In-FEEP Plasmadiagnostics", Space Propulsion, 2003.

[4]C. Böhm and J. Perrin, "Retarding-field analyzer for measurements of ion energy distributions and secondary electron emission coefficients in low-pressure radio frequency discharges", Review of Scientific Instruments 64, 31 (1993).

[5]Y. Sakai and I. Katsumata, "An energy resolution formula of a three plane grids retarding field energy analyzer", Japanese Journal of Applied Physics, 24(3R):337, 1985.

[6]M. Ya-li, T. Fu-jun, X. Yu-xiong, C. Yi-feng, G. Xin, W. Yi, T. Kai and Y. Ze-dong, "Retarding Potential Analyzer Design and Result Analysis for Ion Energy Distribution Measurement of the Thruster Plume in the Laboratory", International Journal of Mechanical, Aerospace, Industrial, Mechatronic and Manufacturing Engineering Vol:6, No:11, 2012.

[7]Z. Zhang, H. Tang, Z. Zhang, J. Wang and S. Cao, "A retarding potential analyzer design for keV-level ion thruster beams", Review of Scientific Instruments 87, 123510 (2016).